

Cold neutrons trapped in external fields

S. Gandolfi,¹ J. Carlson,¹ and Steven C. Pieper²

¹*Theoretical Division, Los Alamos National Laboratory, Los Alamos, NM 87545*

²*Physics Division, Argonne National Laboratory, Argonne, IL 61801*

The properties of inhomogeneous neutron matter are crucial to the physics of neutron-rich nuclei and the crust of neutron stars. Advances in computational techniques now allow us to accurately determine the binding energies and densities of many neutrons interacting via realistic microscopic interactions and confined in external fields. We perform calculations for different external fields and across several shells to place important constraints on inhomogeneous neutron matter, and hence the large isospin limit of the nuclear energy density functionals that are used to predict properties of heavy nuclei and neutron star crusts. We find important differences between microscopic calculations and current density functionals; in particular the isovector gradient terms are significantly more repulsive than in traditional models, and the spin-orbit and pairing forces are comparatively weaker.

PACS numbers: 21.30.-x, 21.60.-n, 21.60.Jz

The properties of inhomogeneous neutron-rich matter are important in both astrophysical and terrestrial regimes. While the equation of state (EOS) and the pairing gap for homogeneous neutron matter have been studied extensively in microscopic theories [1–4], inhomogeneous neutron matter has received comparably little attention. Understanding the inner crust of neutron stars, which affects transient stellar cooling and determine oscillation modes requires knowledge of inhomogeneous neutron-rich matter [5–7]. Neutron-rich nuclei are also the subject of intense theoretical and experimental investigations, driven by their relevance for r-process nucleosynthesis as well as the intrinsic interest in the properties of nuclei at large isospin; [8, 9] they are the principal thrust of rare-isotope accelerators [10].

Simulations of both the crust of neutron stars and of large neutron-rich nuclei employ nuclear energy density functionals fit to nuclei. These density functionals have proved to be extremely successful in describing many nuclei, but involve large extrapolations to reach inhomogeneous neutron matter. To test these extrapolations, we perform calculations of neutron drops – neutrons confined by artificial external fields and interacting via realistic two- and three-nucleon forces. We vary substantially the number of neutrons as well as the strength and shape of the external fields to test the density functional.

The EOS of homogeneous neutron matter has often been included as a constraint to density functional theories (eg. [11]); our objective is to allow inhomogeneous neutron matter to be employed in a similar manner. We find, for example, that once the bulk terms are fixed from the neutron matter EOS, the closed shells of neutrons are primarily sensitive to the gradient terms in the density functional. These pure neutron matter gradient terms have modest effects on nuclei, and hence they are not well constrained in fits to nuclear masses [12, 13]. The closed-shell systems are nearly independent of spin-orbit and pairing terms, but ground and excited states of a single neutron outside a closed shell, or of a single neu-

tron hole, are a sensitive probe of the spin-orbit interaction. Mid-shell results are sensitive to both spin-orbit and pairing terms. We compare our calculated results to several “standard” Skyrme models, and also to a model in which the isovector terms are adjusted to reproduce the ab-initio calculations; these changes are expected to have only a small effect on the nuclear energies used to fit the original parameters. The goal of these studies is to determine which terms in the density functional can be probed through microscopic calculations, and how the adjusted values compare to traditional models. A realistic improved density functional will require a complete refitting of nuclear properties along with the properties of homogeneous and inhomogeneous neutron matter [14, 15].

Interaction and Methods: We report calculations of neutrons in harmonic oscillators (HO) of two frequencies and a Woods-Saxon (WS) well. The full Hamiltonian is:

$$H = -\frac{\hbar^2}{2m} \sum_i \nabla_i^2 + \sum_i V_i + \sum_{i<j} V_{ij} + \sum_{i<j<k} V_{ijk},$$

where $V_i = (m\omega^2/2)r_i^2$ (HO) or $V_i = -V_0/(1 + \exp[(r_i - r_0)/a])$ (WS) with $V_0 = -35.5$ MeV, $r_0 = 3$ fm and $a = 1.1$ fm, and $\hbar^2/m = 41.44$ MeV·fm². The neutron-neutron potential V_{ij} is AV8' [16], a slightly simplified version of the AV18 potential [17]; we find less than 0.25% differences in neutron-drop energies for these two potentials. We also add the Urbana IX model (UIX) [16] three-nucleon interaction (TNI), including the p-wave two-pion exchange (Fujita-Miyazawa) TNI and a short-range phenomenological repulsion. We use this combination of two- and three-nucleon interactions because it produces an EOS consistent with known neutron star masses [1], and because several present-day Skyrme models have used this EOS to constrain the properties of homogeneous neutron matter. Further studies with different interaction models will be valuable, in particular to look at the spin-orbit interactions which might be increased with a three-pion exchange TNI as in Illinois-7 [18].

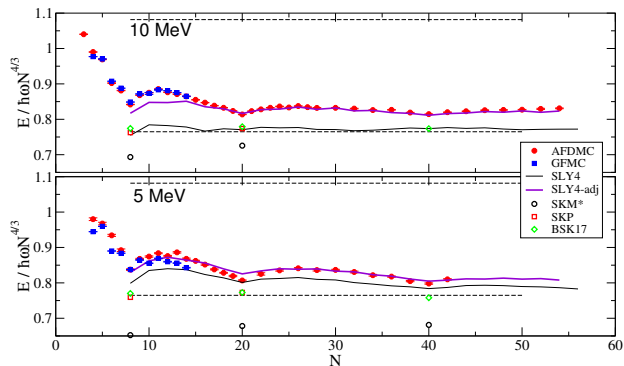


FIG. 1. (color online) Energies divided by $\hbar\omega N^{4/3}$ for neutrons in HO fields with $\hbar\omega = 10$ MeV (top) and 5 MeV (bottom). Filled symbols indicate ab initio calculations; the dashed lines are Thomas-Fermi results (see text); the lower curves are from the SLY4 interaction and the upper curves show the modified SLY4 interaction described in the text.

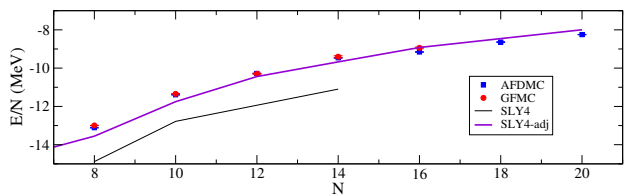


FIG. 2. (color online) Energies per particle for neutrons in the Woods-Saxon field, symbols as in Fig. 1.

Calculations are performed using Green’s Function Monte Carlo (GFMC) [19] and Auxiliary Field Diffusion Monte Carlo (AFDMC) [20] quantum Monte Carlo (QMC) methods. These algorithms evolve an initial trial state, Ψ_T , in imaginary time to yield the ground-state. GFMC sums explicitly over spin and isospin states, and can use very sophisticated Ψ_T [16]. However it is limited to small systems, up to 16 neutrons. In addition to sampling the spatial integrals as in GFMC, AFDMC also samples the spin and isospin degrees of freedom, and hence it can treat larger systems [3]. Both methods use a constraint involving the overlap with Ψ_T to eliminate the Fermion sign problem, and hence are approximate. Studies of light nuclei and neutron matter show they give results within 1% of the exact ground-state energy.

We use external fields yielding low or moderate densities. However, even at small densities neutrons are strongly interacting and pairing can be important. Recent microscopic calculations of neutron matter give s-wave pairing gaps of several MeV [4, 21]. One- and two-nucleon properties including pairing gaps and spin-orbit splittings can be more sensitive to models of the three-nucleon interaction. Calculations of very small neutron drops ($N=6,7,8$) have been performed previously [22–24]. Even these calculations indicated a substantial difference with traditional Skyrme models, which overbind the drops and give too-large spin-orbit splitting.

N	J^π	$\hbar\omega = 5$ MeV		$\hbar\omega = 10$ MeV	
		GFMC	AFDMC	GFMC	AFDMC
7	$1/2^-$	59.17(1)	59.7(2)	118.95(3)	118.01(9)
7	$3/2^-$	59.73(1)	60.3(2)	121.08(3)	120.57(7)
8	0^+	67.01(1)	67.0(2)	135.76(4)	134.7(1)
9	$5/2^+$	81.20(3)	81.6(2)	163.2(1)	162.5(1)
9	$3/2^+$		82.3(2)		166.1(1)
10	0^+	92.1(1)	94.2(2)	188.1(6)	188.5(1)
12	0^+	118.1(1)	120.3(3)	242.0(6)	240.8(1)
13	$5/2^+$	131.5(1)	135.4(3)	267.6(6)	266.3(2)
13	$3/2^+$				269.3(2)
14	0^+	142.2(1)	146.4(3)	291.9(2)	291.7(2)
20	0^+		219.0(4)		441.7(4)
40	0^+		545.8(1.3)		1114.3(9)

TABLE I. Selected energies from GFMC and AFDMC calculations using AV8’+UIX with HO external fields.

Results: The ground-state energies versus neutron number N for the HO potentials are given in Fig. 1 and for the WS potential in Fig. 2. Up to $N=16$ both GFMC and AFDMC results are included. They agree very well for the 10-MeV HO interaction, while for $\hbar\omega = 5$ MeV, the AFDMC results are slightly higher than the GFMC; the maximum difference is 3%, and more typically results are within 1%. The bigger difference for the lower density 5-MeV drops presumably arises because the AFDMC Ψ_T does not yet include pairing, while the GFMC does.

In addition to the microscopic calculations, results for several different Skyrme models are shown in Fig. 1. We also show results for Thomas-Fermi local density approximations [25] using $E(\rho_n)/N = \xi(3/5)(\hbar^2/2m)(3\pi^2\rho_n)^{2/3}$; the upper horizontal line is for free particles, $\xi = 1$, and the lower has $\xi = 0.5$, a reasonable approximation to the EOS of low-density neutron matter. For the 10-MeV well, the density functionals give energies significantly below the Monte Carlo results for all N . The energies are also lower for the 5-MeV well, but less so. This overbinding is a general feature of all the Skyrme models considered. It is intriguing that these same Skyrme models underbind the properties of very dilute neutron systems, typically they are fit to the neutron matter EOS at $\rho = 0.04$ fm $^{-3}$ and above.

Since the Skyrme homogeneous neutron matter EOS have been fit to various microscopic calculations, this overbinding suggests that the gradient terms in inhomogeneous neutron matter should be more repulsive. The observed differences between ab-initio results and the Skyrme functionals are much larger than the differences between experiments and Skyrme models in nuclei, as expected, because of the large extrapolations to inhomogeneous neutron matter.

Isvector Gradient Contributions: As is apparent in Fig. 1, for harmonic oscillators there are closed shells at $N=8, 20$, and 40 neutrons. These closed-shell states are almost exclusively sensitive to the neutron matter

EOS and the isovector gradient terms; pairing and spin-orbit play nearly no role. Hence they are direct probes of the gradient terms; to examine them we have altered the isovector gradient terms in the SLY4 interaction [11] to approximately reproduce the QMC results using a modified version of the ev8 code [26]. The gradient terms are adjusted without changing any isoscalar ($T=0$) parameters or the homogeneous neutron matter EOS.

The lowest-order gradient contribution to the energy density for inhomogeneous matter is $G_d[\nabla\rho_n]^2$. The constants G_d are small and often negative, for example, $G_d = -16, -7, 17, -17, -7$ MeV-fm⁵ for the SLY4, SLY7, BSK17, SkM*, and SkP interactions. Repulsive gradient terms for neutron matter are to be expected on rather general grounds, and are required for the absolute stability of uniform matter in the absence of a background field. The adjusted interaction SLY4-adj gives $G_d = 26.5$, a similar adjustment to the BSK17 interaction which is more attractive for homogeneous neutron matter yields $G_d = 64$. A single adjustment of G_d markedly improves the agreement with QMC results for both the HO and WS fields. A precise fit to both neutron matter and these results would require a more general form of the density functional.

Isovector Spin-Orbit: By examining neutron numbers slightly away closed shells, we can constrain the spin-orbit interaction for neutron drops. For example, $N = 7, 9$ results are sensitive to the spin-orbit interaction, but not to the pairing terms. We find the spin-orbit interaction to be small in the calculated drops; the energies for some low-lying spin-orbit partners are given in Table I.

Small spin-orbit splitting had been found previously in calculations of $N=7$ drops and our results show similar effects for all systems near closed shells ($N=7,9,11,\dots$). The simplest (standard) Skyrme parametrizations give a strength ratio of 3:1 between isoscalar ($T = 0$) and isovector ($T = 1$) spin-orbit couplings. We find an even smaller isovector coupling, approximately 1/6 of the isoscalar coupling, reproduces the ab initio calculations. The combined factor of 1/6 is in reasonable agreement with 1/8 found in a diagrammatic examination of spin-orbit splittings from microscopic interactions [27], and with results obtained in an examination of Skyrme parameters from Pb isotopes [28]. Relativistic mean fields yield zero strength in the isovector channel [29], while recent results from the pion contribution from chiral interactions give nearly equal isovector and isoscalar strengths [30].

Isovector Pairing: The mid-shell results (eg. $N=14, 30$) and odd-even staggerings are sensitive to the pairing interactions as well as the spin-orbit force. Fixing the spin-orbit strength from near closed-shells, we adjust the pairing strength to fit the calculated spectra. There is a significant interplay between the pairing and spin-orbit forces required to reproduce microscopic calculations. A small spin-orbit force results in many quasi-degenerate levels which enhances pairing in mid-shell systems.

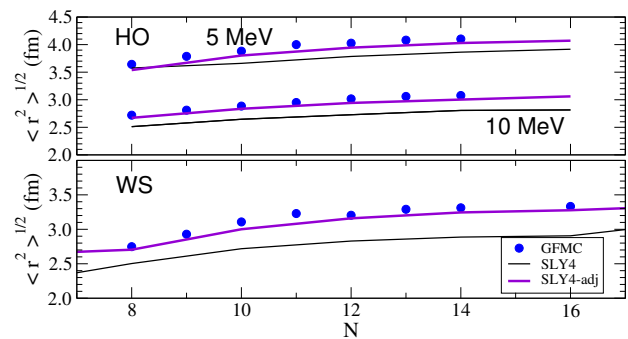


FIG. 3. (color online) Calculated radii of neutrons confined in HO (upper) and WS (lower), fields compared to original and adjusted Skyrme models (see text).

Several models of pairing are used in density-functional theories. We employ a simple volume parametrization with a delta-function spatial dependence, a density cutoff that restricts pairing to $\rho_n < \rho_0$, and limit the pairing to single-particle orbitals less than 5 MeV from the Fermi energy. We find a reduction from a typical 1 GeV-fm³ strength to half that value significantly improves agreement with microscopic results. A reduction of pairing in neutron-rich nuclei has recently been found to give a better fit to experimental energy differences of 156 nuclei of mass $A=118$ to 196 [31].

Adjusting these three parameters (gradient term $G_d = 26.5$, spin-orbit coupling = 123 MeV-fm³ and pairing strength = 500 MeV) in the density functional increases the agreement across all external fields and all particle numbers. This is shown by the upper solid curves (SLY4-adj) in Fig. 1.

Radii and Mass Distributions: Our calculations yield precise estimates for RMS radii and the density distributions of the smaller drops. The average densities, defined as $\int d^3r \rho_n^2(r)/N$, of the drops in the 5-MeV HO well are approximately 0.02 fm⁻³, or about 1/8 nuclear matter saturation density, while for the 10-MeV HO and the WS wells they are ~ 0.045 fm⁻³, or almost 1/3 nuclear matter saturation density.

The RMS radii obtained in microscopic calculations are compared with the original and adjusted Skyrme density functional results in Fig. 3. The density distributions for $N=8$ and 14 are compared in Fig. 4. Since we are comparing gross properties of inhomogeneous matter, we plot the densities weighted with the phase space: $r^2\rho_n(r)$, which gives a better picture of the density distributions near the average density of the system. In every case the adjusted Skyrme interaction produces a better description of the radii and density distributions. The $N = 8$ calculations depend primarily upon the gradient terms, the reduction in pairing and spin-orbit are also important for $N = 14$. The improvement in the mid-shell $N=14$ case is particularly dramatic, as a significant shift in the density occurs with the modified isovector Skyrme

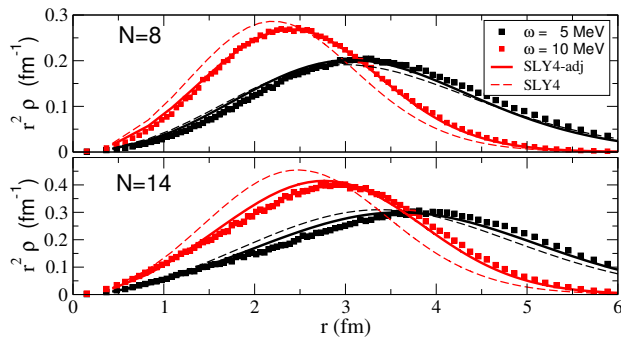


FIG. 4. (color online) Calculated densities of neutrons in HO potentials, compared to Skyrme models (see text).

parameters, bringing the results into much better agreement with microscopic calculations.

Conclusions: We have examined the properties of neutrons confined in external fields to study the properties of inhomogeneous neutron matter. These ab-initio calculations place significant constraints on the nuclear energy density functional in a regime far from that probed by fitting to available nuclei. They indicate the need for more repulsive gradient terms in pure neutron matter, and a reduced isovector spin-orbit and pairing strength compared to standard functionals. With a combined fit of density functionals to both nuclei and neutron matter, more reliable predictions should be possible for very neutron-rich nuclei including those participating in r-process nucleosynthesis. These improved functionals would also be extremely valuable in examining the neutron skin thickness of lead [32], as can be probed in parity-violating electron scattering. Much more reliable predictions for extremely neutron-rich astrophysical environments can also be expected. The numerical values of the results shown in the figures are given in Ref. [33].

We thank G. F. Bertsch, A. Bulgac, S. a Beccara, J. Dobaczewski, W. Nazarewicz, P. Maris, F. Pederiva, S. Reddy, J. Vary, and R. B. Wiringa for valuable discussions. We are indebted to K. E. Schmidt for providing us the AFDMC code. This work is supported by the U.S. Department of Energy, Office of Nuclear Physics, under contracts DE-FC02-07ER41457 (UNEDF SciDAC), DE-AC02-06CH11357, and DE-AC52-06NA25396. Computer time was made available by Argonne's LCRC, the Argonne Mathematics and Computer Science Division, Los Alamos Open Supercomputing, the National Energy Research Scientific Computing Center (NERSC) and by a DOE INCITE grant on the Argonne BG/P.

- [2] D. J. Dean and M. Hjorth Jensen, *Rev. Mod. Phys.* **75**, 607 (2003).
- [3] S. Gandolfi *et al.*, *Phys. Rev. C* **79**, 054005 (2009); *Mon. Not. R. Astron. Soc.* **404**, L35 (2010).
- [4] A. Gezerlis and J. Carlson, *Phys. Rev. C* **77**, 032801 (2008); *Phys. Rev. C* **81**, 025803 (2010).
- [5] D. G. Ravenhall, C. J. Pethick, and J. R. Wilson, *Phys. Rev. Lett.* **50**, 2066 (1983).
- [6] P.S. Shternin *et al.*, *Mon. Not. R. Astron. Soc.* **382**, L43 (2007).
- [7] E. F. Brown and A. Cumming, *ApJ* **698**, 1020 (2009).
- [8] J. Dobaczewski *et al.*, *Phys. Rev. C* **53**, 2809 (1996).
- [9] J. Dobaczewski *et al.*, *Prog. Part. Nucl. Phys.* **59**, 432 (2007).
- [10] D. F. Geesaman *et al.*, *Annu. Rev. Nucl. Part. Sci.* **56**, 53 (2006).
- [11] E. Chabanat *et al.*, *Nucl. Phys.* **A627**, 710 (1997); *Nucl. Phys.* **A635**, 231 (1998); *Nucl. Phys.* **A643**, 441(E) (1998).
- [12] R. J. Furnstahl, B. D. Serot, *Nucl. Phys.* **A671**, 447 (2000).
- [13] B. A. Brown, *Phys. Rev. C* **58**, 220 (1998) and references therein.
- [14] See UNEDF SciDAC project, www.unedf.org.
- [15] G. F. Bertsch, B. Sabbey, and M. U. Usnakki, *Phys. Rev. C* **71**, 054311 (2005).
- [16] B. S. Pudliner *et al.*, *Phys. Rev. C* **56**, 1720 (1997).
- [17] R. B. Wiringa, V. G. J. Stoks, and R. Schiavilla, *Phys. Rev. C* **51**, 38 (1995).
- [18] S. C. Pieper, *AIP Conf. Proc.* **1011**, 143 (2008).
- [19] S. C. Pieper, R. B. Wiringa, and J. Carlson, *Phys. Rev. C* **70**, 054325 (2004), and references therein.
- [20] K. E. Schmidt, S. Fantoni, *Phys. Lett. B* **446**, 99 (1999).
- [21] S. Gandolfi *et al.*, *Phys. Rev. Lett.* **101**, 132501 (2008); *Phys. Rev. C* **80**, 045802 (2009).
- [22] B. S. Pudliner *et al.*, *Phys. Rev. Lett.* **76**, 2416 (1996).
- [23] A. Smerzi, D. G. Ravenhall, and V. R. Pandharipande, *Phys. Rev. C* **56**, 2549 (1997).
- [24] F. Pederiva *et al.*, *Nucl. Phys.* **A742**, 255 (2004).
- [25] S. Y. Chang and G. F. Bertsch, *Phys. Rev. A* **76**, 021603(R) (2007).
- [26] P. Bonche *et al.*, *Nucl. Phys.* **A43**, 39 (1985).
- [27] N. Kaiser, *Phys. Rev. C* **70**, 034307 (2004).
- [28] P.-G. Reinhard and H. Flocard, *Nucl. Phys.* **A584**, 467 (1995).
- [29] M. Onsi *et al.*, *Phys. Rev. C* **55**, 3166 (1997).
- [30] N. Kaiser, *Eur. Phys. J. A* **45**, 61 (2010).
- [31] M. Yamagami, Y. R. Shimizu, and T. Nakatsukasa, *Phys. Rev. C* **80**, 064301 (2009).
- [32] P. G. Reinhard and W. Nazarewicz, *Phys. Rev. C* **81**, 051303 (2010).
- [33] See supplementary material at [URL will be inserted by AIP] for numbers reported in the figures.

[1] A. Akmal, V. R. Pandharipande, and D. G. Ravenhall, *Phys. Rev. C* **58**, 1804 (1998).